Virginia Institute of Marine Science Report CHSD-2019-01.
https://www.vims.edu/people/friedrichs_ct/cv/chsd-2019-01.pdf

Fractal floc properties in estuarine surface waters: Insights from video settling, LISST, and pump sampling

Kelsey Fall[1, 2], Carl Friedrichs[1], Grace Massey[1], David Bowers[3], and Jarrell Smith[2]
[1]Virginia Institute of Marine Science, Gloucester Point, VA 23062, USA
[2] U.S. Army Engineer Research and Development Center, Vicksburg, MS, USA
[3] Bangor University, Menai Bridge, United Kingdom

Abstract

Two definitions of floc density are frequently used when characterizing floc properties: (1) excess density = $\Delta\rho$, determined from floc diameter (d_f) and settling velocity, and (2) apparent density = ρ_a, determined from floc bulk volume and filtered samples of total suspended solids (TSS). If one assumes fractal flocs are aggregates composed of interstitial water combined with primary particles of diameter, d_p, and density, ρ_p (which contain no water), and that a given fractal dimension and (F) and ρ_p yields a specific $\Delta\rho$ for a given d_f, a quantitative relationship between excess density ($\Delta\rho$) and apparent density (ρ_a) can be used to estimate ρ_p and d_p. Another key measure of sediment density is (3) the dry density of filtered solids = $\rho_{TSS,}$ calculated from the TSS organic fraction, F_{org}. If a single population of fractal flocs dominates a suspension, it follows from fractal theory that ρ_p as estimated above should be nearly equal to ρ_{TSS}, and the consistency of ρ_p and ρ_{TSS} can be used as a check on the validity of the fractal assumption. This novel set of calculations was applied to observations of near-surface particle properties collected in the York River estuary in fall 2014, 2015 and 2016 using a profiling system equipped with a Laser In-Situ Scattering and Transmissometry (LISST) 100X, a high-definition Particle Imaging Camera System (PICS) incorporating a video settling tube, and a high-speed pump sampler. When fractal flocs were present (i.e. $\rho_p \approx \rho_{TSS}$), suspensions with lower F_{org} were composed of smaller, denser primary particles. In contrast, suspensions with higher F_{org} (i.e., lower ρ_{TSS}) were composed of larger, less dense primary particles. Floc fractal dimension (F) did not show a very strong of a relationship with F_{org}, suggesting it may not be as important to constrain as d_p and ρ_p when assuming a fractal model. Alternatively, when ρ_p was not consistent with ρ_{TSS}, it was concluded that simple fractal behavior could not describe the floc populations present.

1. Introduction

The properties of particles in surface waters are especially important to the fate of incident light, with direct ramifications for primary production, habitat and water quality, and optical remote sensing. Typical near surface estuarine particles are not single solid particles, but clusters of inorganic and organic particles and water, called flocs. Scattering of light by estuarine flocs depends directly on floc size (d_f) and density (ρ_f) (Bowers et

al., 2011). Due to the fragile nature of flocs, in situ sampling is required to accurately characterize d_f and ρ_f, however obtaining such measurements is often quite difficult (Winterwerp and Van Kesteren, 2004). The most popular ways to approximate ρ_f is thru fractal relationships. Kranenburg (1994) used the fractal approach to establish a mathematical relationship to relate floc size (d_f) and density (ρ_f) to the size (d_p) and density (ρ_p) of the fractal constituents or primary particles using a dimensionless parameter, referred to a fractal dimension (F). d_p, ρ_p, and F are quite difficult to constrain for natural suspensions (Fettweis, 2008). Fortunately, F can be derived by fitting a power law function to d_f and settling velocity (w_s) or d_f and ρ_f at all scales of d_f, simplified as $w_s \sim d_f^{F-1}$ and $\rho_f \sim d_f^{3-F}$. Power law fractal relationships are inferred from in situ measurements of settling velocity (w_s) and/or inferred excess density ($\Delta\rho$) and d_f with video imaging systems equipped with a settling column (Dyer and Manning, 1999; Sanford et al., 2005; Smith and Friedrichs, 2015) or from measuring the ratio of suspended mass concentration to suspended volume concentration determined by an optical or laser diffraction based particle sizing instrument (apparent density, ρ_a) and some approximation of floc size, commonly median diameter by volume, d_{50} (Mikkelsen and Pejrup, 2001; Sanford et al., 2005, Bowers et al., 2009; Hurley et al., 2016).

Compared with flocs in the bottom boundary layers, the fractal nature of flocs in estuarine surface waters has been studied in situ relatively less, and it has yet to be established whether fractal models are appropriate for such suspensions. There are many more challenges associated with collecting in-situ observations of floc properties of surface suspensions. These include the motion of observing platforms, lower particle concentrations, smaller particles, lower settling velocities, and lower contrast in optical imaging. Video settling systems and particle imaging cameras generally have limited size resolution, most requiring particles to be at least 3 pixels or larger for accurate tracking for size and settling velocity (Sanford et al., 2005; Smith et al., 2011; Hill et al., 2011). In addition, video settling systems generally require a stable platform to ensure estimates of w_s are not influenced by background fluid velocity. The Laser In-Situ Scattering and Transmissometry (LISST) series produced by Sequoia Scientific are popular laser diffraction instruments for measuring in situ particle size distributions, resolving small particles down to $d_f \sim 1.25\text{-}2.5$ μm (Agrawal and Perjup, 2000). Although LISST

instruments are capable of resolving smaller flocs relative to camera and video systems, they cannot directly measure density of settling velocity. Particles in the surface water in estuarine and coastal environments tend to contain a relatively larger fraction of organic matter, so assumptions inferred from the analysis of inorganic flocs (near the bed) may not hold for near surface flocs. For example, because of the larger contribution of organic matter the changes in density and size may be more dramatic than for inorganic flocs and the fractal dimension may not be as close to 2 (Winterwerp and van Kesteren, 2004; Braithwaite et al., 2010; Hill et al., 2011). Also, the density of the primary building blocks of organic-rich flocs may be significantly less than the commonly assumed inorganic value of ~2300-2600 kg/m^3 (Khelifa and Hill; 2006; Fettweis, 2008).

Recently, a new approach that combines the relationship between excess density ($\Delta\rho$) and apparent density (ρ_a) and with Kranenburg's (1994) fractal size-excess density relationship has been used characterize fractal dimension and primary particle properties (Ganju et al., 2007; Braihtwaite et al., 2010; Bowers, et al., 2017; Chapalain et al., 2018). Excess density is related to the fractal nature of particles where apparent density associated with the measurements of volume concentration distribution. They are related to one another by primary particle density (Hurley and Hill, 2016). Kranenburg's (1994) fractal size-excess density relationship states that a given fractal dimension, primary particle size and density will yield a specific excess density ($\Delta\rho$) for a corresponding floc size (d_f). If you assume the fractal size-excess density relationship, mass concentration can be estimated from the volume distribution using the quantitative relationship between excess density ($\Delta\rho$) and apparent density (ρ_a). Comparing predicted mass concentrations to observed mass concentrations yields predictions for fractal dimensions and primary particle characteristics. Ganju et al., 2007 found that assuming a fractal dimension of 2 and primary particle size of 2 microns, produced estimated mass concentrations that were consistent with observed concentrations throughout San Francisco Bay. Braithwaite et al., 2010 used the relationship to define a representative primary particle size and density for the Tamar Estuary, 1787 kgm^{-3} and 3.9 microns, and then used those values to estimate fractal dimensions throughout the system. She concluded that the relationship is fairly robust and useful to predict primary particle size and density from particle size distributions and mass concentrations. Bowers et al., 2017 and Chapalain et al., 2018

assumed a constant ρ_p and d_p and estimated F. Though these applications have shown how useful these relationships are to quantify fractal and primary particle characteristics, the approach is still somewhat constrained. It requires assumptions regarding F or ρ_p and d_p or all three. Additionally, all three are dependent on one another, which adds built-in bias to the results as well as hinders any validation.

The goal of this paper is to gain insight into the fractal properties of small, organic-rich flocs in estuarine surface waters, which have received considerably less attention. This project combined observations collected using a high-resolution particle imaging video system equipped with a settling column with a Sequoia Scientific LISST-100X to better characterize the properties of estuarine surface flocs. Automated in situ video settling tube analysis was employed to confidently assess the size and settling velocity (thus density) of 10s of thousands of flocs and determine well-constrained estimates of fractal dimension. The quantitative relationship between $\Delta\rho$ and ρ_a and the fractal size-density relationship were combined with independent "in-situ" estimates of fractal dimensions, observations of particle size distributions, total suspended solids to quantify fractal primary particle density and size, and a novel approach to validate the fractal model inferred from video settling analysis is introduced.

Table 1: Description of Symbol Notations used in this paper.

Symbol	Meaning	Units
$\Delta\rho$	Floc excess density (flocs's wet density minus the density of water)	kg/m^3
ρ_a	Floc apparent density (floc's dry mass divided by its wet volume)	kg/m^{-3}
ρ_f	Floc wet density	kgm^{-3}
M_f	Total floc wet mass	kg
M_p	Total mass of primary particles (solids) within a floc	kg
M_w	Total mass of water within a floc	kg
V_f	Total floc volume	m^3
V_p	Total volume of primary particles (solids) within a floc	m^3
V_w	Total volume of water within a floc	m^3
ρ_w	Density of water	kg/m^3
ρ_p	Primary particle density	kg/m^3
ρ_{tss}	Primary Particle density inferred from TSS and F_{org} (Eqn. 3f)	kg/m^3
d_p	Primary particle diameter	µm
d_f	Floc diameter	µm
F	Fractal dimension	
g	Gravitational acceleration, ~ 9.8	m/s^2
υ	Kinematic viscosity	m^2/s^1
w_s	Floc settling velocity	mm/s
TSS	Total suspended mass (solids) determine from pump samples	mg/L
TSS_p	Fractal estimated mass concentration from PSDs	mg/L
F_{org}/F_{inorg}	Bulk organic/inorganic fraction of pump samples TSS	
ρ_{org}/ρ_{inorg}	Density of organic/inorganic solids	kg/m^3
$F_{40\text{-}100\mu m}$	Fractal dimension fit from PICS for particles with 40 µm ≤ d_f ≤ 100 µm	
$F_{>100\mu m}$	Fractal dimension fit from PICS for particles with d_f >100 µm	
α	Scaling factor for PICS volume concentration	
$VC_{LISSSTi}$	LISST-100X volume concentration in size class bin i	µL/L

VC_{PICSi}	PICS volume concentration in size class bin i	mm^3

2. Theoretical Background

2.1 Definitions of Δρ and ρ_a

Excess density (Δρ) and apparent density (ρ_a) are two related definitions of particle density that are each commonly utilized when characterizing floc properties. Excess density, which is a floc's wet density minus the density of water, appears in particle settling relationships that balance a particle's effective submerged weight against frictional drag as a particles settles. Video settling tubes are often used to estimate Δρ through direct measurements of particle settling velocity (e.g., Fennessy et al., 1994; Hill et al., 1998; Manning and Dyer, 1999; Hill et al., 2011; Smith and Friedrichs, 2011; Smith and Friedrichs, 2015). In contrast, apparent density (ρ_a) is a floc's dry mass divided by its wet volume. Typically, measurements of dry mass concentration determined by filtration, combined with estimates of total wet floc volume, provide bulk estimates of ρ_a (e.g., Mikkelsen and Perjrup, 2001; Bowers et al., 2009; Braithwaite et al., 2010; Bowers et al., 2011; Hurley and Hill, 2016). If one assumes flocs are aggregates composed of interstitial water combined with primary particles of uniform density (which contain no water), then it is relatively straightforward to derive a quantitative relationship between Δρ and ρ_a.

2.2 Relationship between Δρ and ρ_a

The quantitative relationship between Δρ and ρ_a follows from the definition of each, re-expressed in terms of the masses and volumes of the component particles and interstitial water (Mikkeslen and Perjup, 2001; Fettweis, 2008; Hurley et al., 2016). A floc's wet density (ρ_f) can be described as the wet mass of the floc (M_f) divided by the volume of the floc (V_f), where M_f is the sum of the mass of the primary particles (M_p) and water (M_w) within the floc, and V_f is the sum of the volume of the primary particles (V_p) and water (V_w). Using these definitions and some algebra, it follows that

$$\Delta\rho = \rho_f - \rho_w = \frac{M_p+M_w}{V_p+V_w} - \frac{M_w}{V_w} = \frac{V_w M_p - V_p M_w}{(V_p+V_w)V_w} \qquad \text{Eqn. 2a.}$$

where $\rho_w = M_w/V_w$ is the density of water. A floc's apparent density (ρ_a) is simply M_p/V_f, which can be expanded as

$$\rho_a = \frac{M_p}{V_p + V_w} \qquad \text{Eqn. 2b.}$$

Dividing Eqn. 2a by 2b then yields

$$\frac{\Delta\rho}{\rho_a} = \frac{V_w M_p - V_p M_w}{V_w M_p} = 1 - \frac{\rho_w}{\rho_p} \qquad \text{Eqn. 2c}$$

where $\rho_p = M_p/V_p$ is the primary particle density. From eqn. 2c, it is evident that the ratio of excess density to apparent density is a function of primary particle density. For a given floc population, this ratio will remain constant across all floc sizes and floc densities if the density of the primary particles is uniform.

2.3 **Use $\Delta\rho$ and ρ_a to estimate ρ_p**

Based on the relationships outlined above, it follows that concurrent, independent measurements of ρ_a and $\Delta\rho$ can together be used to estimate the primary particle density (ρ_p) for a given floc population. If independent observations of $\Delta\rho$ and ρ_a confirm a stable ratio between $\Delta\rho$ and ρ_a across a range of floc sizes, then that stable ratio of $\Delta\rho$ to ρ_a can be used to directly estimate ρ_p via Eqn. 2c. This method for estimating ρ_p does not require any assumptions regarding the fractal nature of the flocculation process. Nor does it assume that the primary particles are of a single size. It only assumes that the densities of the primary particles are uniform within a given floc. Unfortunately, obtaining independent in situ measurements of both ρ_a and $\Delta\rho$ for individual flocs is quite difficult. Advances in video settling tubes have made it easier to obtain measurements of $\Delta\rho$, but often the best that can be done to obtain a second independent measurement of apparent density is measure a bulk or average value to characterized ρ_a. However, if one assumes a fractal model, the relationship between a bulk ρ_a or a bulk $\Delta\rho$ can be used to estimate the primary particle density (ρ_p).

2.4 Fractals, $\Delta\rho$ and ρ_a

The constant ratio between $\Delta\rho$ and ρ_a derived above also means that for flocs that do conform to classical fractal relations, the same fractal dimension will describe the dependence of both $\Delta\rho$ and ρ_a on floc size. Self-similar fractal theory was originally applied to $\Delta\rho$ by Kranenburg (1994), yielding

$$\Delta\rho = \rho_f - \rho_w = \left(\rho_p - \rho_w\right)\left[\frac{d_p}{d_f}\right]^{3-F} \qquad \text{Eqn. 2d}$$

where d_p and d_f are the primary particle and floc diameters, and F is the floc fractal dimension. In deriving Eqn. 2d, Kranenburg (1994) assumed that primary particles in a given fractal floc population are of a single size, d_p, as well as a single density, ρ_p, and yield a specific excess density ($\Delta\rho$) for a corresponding floc size (d_f).

Using Eqn. 2c to eliminate $\Delta\rho$ in Eqn. 2d immediately yields

$$\rho_a = \rho_p\left[\frac{d_p}{d_f}\right]^{3-F} \qquad \text{Eqn. 2e}$$

The above results are consistent with the approach of other authors who have previously assumed that either $\Delta\rho$ (Hill et al., 1998; Dyer and Manning, 1999; Fettweis, 2008; Hill et al., 2011) or ρ_a (Mikkelsen and Perjup, 2001; Braithwaite et al., 2010; Hill et al., 2013; Bowers et al., 2017) individually obeys a fractal relation, with F representing the flocs' characteristic fractal dimension in either case. Based on Eqns. 2d and 2e, and assuming one is sampling a population of self-similar flocs, it follows that estimates of either $\Delta\rho$ or ρ_a, can be used to determine F via a local best-fit log-log regression against observations of d_f.

Assuming particles are nonabsorbent spheres, the total mass concentration (TSS) can be predicted from summing the apparent density, ρ_a (Eqn. 2b), multiplied by volume concentration (VC) over all size class bins (i) of the PSD (Ganju et al., 2007; Braithwaite et al., 2010):

$$TSS_p = \frac{M_p}{V_w} = \sum_{d_{min}}^{d_{max}}\left\{\frac{M_p}{V_p+V_w}\right\}_i\left\{\frac{V_p+V_w}{V_w}\right\}_i = \sum_{d_{min}}^{d_{max}}\{\rho_a\}_i\{VC\}_i \qquad \text{Eqn. 2f.}$$

Rearranging Eqn. 2e, ρ_a, in Eqn. 2f can be expressed in terms of $\Delta\rho$, ρ_w, and ρ_p:

$$\rho_a = \Delta\rho\left(\frac{1}{1-\frac{\rho_w}{\rho_p}}\right) \qquad \text{Eqn. 2g.}$$

If one assumes a fractal model (Eqn. 2d, 2e) values for ρ_p, estimated by matching PSD-estimated TSS (TSS_p) to observed TSS from pump samples (Ganju et al., 2007; Braithwaite et al., 2010).

2.5 Use $\Delta\rho$ and ρ_a to estimate d_p

Having already used observations of $\Delta\rho$ and ρ_a to estimate ρ_p, via Eqn. 2c, then a local best-fit of observations to either Eqn. 2d or Eqn. 2e can be used to estimate the primary particle size (d_p) most consistent with the assumed fractal model. If one extrapolates Eqns. 2d and 2e toward the extreme of the smallest possible flocs, i.e., where $d_f = d_p$, then one finds

$$\rho_a = \rho_p = \Delta\rho + \rho_w \quad \text{at} \quad d_f = d_p \qquad \text{Eqn. 2f}$$

In other words, for the simplest fractal case, where d_p, ρ_p and F remain constant across all floc sizes, the difference between the apparent density and excess density for the primary particles is exactly the density of water. Note that "water" here may be brackish or saline and is not restricted to exactly 1000 kg/m^3. Also, no assumptions have yet been made regarding the composition of the primary particles. For example, the characteristic primary particle could be a tightly bound combination of inorganic and organic matter with a density ranging anywhere between ~1000 and ~2700 kg/m^3.

3. Methods

3.1 In-situ Sampling and Instrumentation

Observations of particle properties were collected in surface waters of the York River estuary (Figure 1) using the Coastal Hydrodynamics and Sediment Dynamics (CHSD) water column profiler (Figure 2). The York is a partially-mixed, microtidal estuary, and spans 50 km from West Point to Gloucester Point (Friedrichs, 2009). The York is an ideal

site to observe flocs with a wide range of characteristics. It exhibits persistent spatial patterns in stratification, physical mixing, suspended sediment and organic matter concentrations along its main axis (Moore et al., 1997; Schaffner et al., 2001; Friedrichs, 2009). The middle to upper York oscillates between partially- and well-mixed conditions, tends to have more intense tidal currents, a greater range of salinities, and higher suspended sediment concentrations (Friedrichs, 2009). A primary estuarine turbidity maximum occurs upstream near West Point and the middle York seasonally experiences the temporary presence of a secondary turbidity maximum (Moore et al., 1997; Friedrichs et al., 2008). In the lower York the estuary deepens and as a result, the water column is generally more stratified, turbulence is weaker, and suspended sediment concentrations are lower (Schaffner et al., 2001).

Mounted on the CHSD profiler is a Sequoia Scientific Laser In-Situ Scattering and Transmissometry instrument Type C (LISST-100X), a high-definition particle imaging camera system (PICS), a YSI6600 conductivity, temperature and depth probe (CTD), and a high-speed pump sampler with an intake hose at roughly the same height as the LISST-100X. At each sampling station, the profiler was deployed off the VIMS R/V Ellis Olsson, lowered to a depth of 1-3 meters below the surface, and kept there while the suite of instruments sampled for 2-5 minutes.

Observations were collected on ten cruises between September and December over the course three years, 2014-2016. Samples were collected in the fall and early winter to avoid phytoplankton blooms, which are most likely to occur during spring and summer in this system (Sin et al., 1999; Reay, 2009). An aim of this study is to examine properties of flocculated particles near the surface without observations being significantly confounded by high the presence of relatively large algal cells. Four of the cruises surveyed six stations along the York from the mouth upriver to the ETM. Each station was sampled once on the same day. For the other six cruises, the vessel was anchored at one station, and samples were collected once an hour for half a tidal cycle (~6 hours), bracketing either a flood or ebb tide. One anchor station was completed in the lower York and the others were done in the middle York, in the general location of the secondary turbidity maximum and the CHSD long-term observing station (Friedrichs et al, 2008;

Cartwright et al, 2009).

3.1.1 Determining floc size (d_f), settling velocity (w_s) and excess density ($\Delta\rho$) using the PICS

The PICS video camera system (Figure 2) was developed to collect in-situ measurements of particle diameter and settling velocity, which are then combined to estimate particle excess density (Smith and Friedrichs, 2011; 2015). The PICS unit utilized here consists of a meter-long settling column with a 5-cm inner diameter, a 1.4 mega-pixel digital video camera, and 1 mm thick, 635 nm laser light sheet (which is significantly thinner than the camera's ~3 mm focal depth). The thin laser sheet optimizes the sharpness of the camera's focus, but it limits the largest size of fully resolved flocs to ~ 1 mm. At each end of the settling column are two pneumatically controlled ball valves used to open and close the settling column. The valves are kept open as the profiler is lowered to the desired sampling depth. The two ball valves are then closed, and water motion within the tube is allowed to dissipate for ~15-30 seconds. A 30-second video is then captured at 8 frames per second. The imaged region within the settling column is approximately 14 mm x 10 mm x 1 mm with a resolution of 1360 x 1024 pixels, i.e., 1 pixel = 10 x 10 microns (Smith and Friedrichs, 2015).

The automated image processing routines developed by Smith and Friedrichs, 2011; 2015 combine particle tracking velocimetry, PTV, with automated particle image velocimetry, PIV, to identify and track particles between successive image frames, estimate background fluid velocity, and measure floc size (d_f) and settling velocity (w_s). Prior to PTV/PIV analysis, greyscale images were converted to binary images using a globally applied greyscale threshold, which was prescribed through meticulous manual inspection of thousands of representative images sequences (Smith and Friedrichs, 2015). Determination of the greyscale threshold through visual inspection is extremely tedious and somewhat subjective, however the pre-existing automated methods for determining a global threshold, specifically Otsu's method (Otsu, 1976) and Linter and Sills, 2006 were determined to not be appropriate for the data collected here. Both were biased towards larger, brighter particles and had the tendency to omit smaller particles. An automated

procedure that efficiently identifies and accurately sizes both large and small flocs, while omitting out of focus particles is currently being developed. Once images were converted into binary format, PTV analysis was applied to size and match particles between adjacent frames. In order to reliably track particles, image processing requires particles to appear in an area of at least 3 x 3 pixels or greater (Milligan and Hill, 1998; Mikkelsen et al., 2004; Lintern and Sills 2006). The PICS minimum resolvable size is 30 microns. PIV assessed the motion of smaller particles (≤ 2 pixels in diameter) via spatial cross-correlation between frames to estimate background fluid velocity. The frame-averaged PIV velocity is then subtracted from each PTV velocity to produce an averaged estimated of w_s for each larger particle. For suspended mass concentrations of flocs on the order of 10 mg/L or more during a typical 30 second video, 1000 or more distinct particles ≥ 30 microns in size are assigned individual w_s values. Concurrent measurements of w_s and d_f estimate excess density ($\Delta\rho$) for each tracked particle by rearranging Soulsby's (1997) empirically derived expression for settling velocity:

$$\Delta\rho = \rho_f - \rho_w = \frac{\rho_w \upsilon^2}{g K_2 {d_f}^3}\left[\left(\frac{w_s d_f}{\upsilon} + K_1\right)^2 - {K_1}^2\right] \qquad \text{Eqn. 3a}$$

where g is gravitational acceleration, υ is kinematic viscosity, and K_1/K_2 are empirical constants (K_1=10.36, K_2=1.049).

The PICS exhibits systematic limitations especially toward smaller particle sizes. The PICS quantifies characteristic d_f and w_s for particles (≥ 30 microns) with statistical rigor by tracking many, many particles (Smith and Friedrichs, 2011, 2015). However, the fraction of the total number of particles present that are successfully tracked is reduced at smaller sizes relative to larger sizes. This is because the larger a particle is, the better its detailed shape is resolved by 10 micron pixels, and the more likely it is to pass the criteria utilized by the PICS to determine whether particles in consecutive video frames match. For a frame-to-frame particle match to be accepted by the PICS, a correlated particle must change in estimated cross-sectional area by no more than 25%, and the ratio of its minor-to-major dimensions must change by no more than 15% (Smith and Friedrichs, 2015). In addition to improving the quality of w_s estimates, these stringent matching criteria also help ensure the size and shape of accepted particles (averaged over at least 5

frames) have been accurately determined. However, it also means that the concentration of smaller particles within the PICS resolution range are underrepresented.

3.1.2 LISST-100X Type C

A Sequoia Scientific Laser In-Situ Scattering and Transmissometry instrument Type C (LISST-100X) was deployed for an additional measurement of particle size, specifically to help account for smaller flocs in suspension. Although the LISST cannot track and measure individual particles, it can be used to resolve reliable particle size distributions (PSDs) in-situ for a range of particle sizes, shapes, and compositions (e.g., Fugate and Friedrichs, 2003; Agrawal et al., 2008; Andrews et al., 2010; Bowers et al., 2011; Cartwright et al., 2011; Hill et al., 2011; Fettweis and Baeye, 2015). The LISST-100/100X emits a collimated beam of light (670 nm) through an in situ sample and measures the intensity of that light that is scattered light on 32 concentric ring detectors. The pattern of scattered light is numerically inverted using an instrument-specific calibration matrix to estimate particle volume concentrations for 32 logarithmically spaced size classes (Agrawal and Pottsmith, 2000). The LISST-100X Type C, which was used in this study, measures the size distribution of volume concentration from 2.5 to 500 microns. At each station, the LISST-100X sampled for bursts of 2 to 5 minutes, coincident in time the collection of PICS data and of water samples. LISST-100X PSDs were collected at 1 Hz and the mean PSD over the duration of the burst was used in subsequent analysis. Sequoia Scientific's random shape scattering property kernel matrix was used to invert the data collected in this study.

When using the LISST-100/100X series of instruments, it is important to be aware of its tendency to produce "rising tails" in estimated volume concentration at the lower-most and upper-most ends of its PSD range. Spurious rising tails at larger particle sizes are relatively common in LISST-100/100X output and can be due either to the presence of larger particles out of range, increased sensitivity of larger particles to refractive index effects, and/or the greater uncertainties inherent in resolving very small scattering angles (Agrawal and Pottsmith, 2000; Mikkelsen et al., 2005). The presence of particles smaller than 2.5 microns tends to increase the volume of particles estimated in the smallest size

classes by the LISST-100X Type C by a magnitude similar to the volume of the out-of-range particles (Andrews et al., 2010). Excess ambient light, which impinges on the LISST-100/100X's outer rings, can also increase the apparent particle volume assigned to the smallest size classes (Reynolds et al., 2010; Andrews et al., 2010), as can the presence of irregularly shaped particles, which scatter at wider angles than do spheres (Agrawal et al., 2008). A LISST-100X Type B was deployed at the CHSD long-term observing station at a depth of approximately 2 meters below the surface, where it sampled for 100 second bursts every 15 minutes. 12 sampling stations in this study were collected adjacent to the Type B at times that overlapped. Overall, PSDs from two instruments agree quite well between ~ 4 and 100 microns. On average, the Type B showed a strong decrease in volume concentrations between 1.25 and 4 microns. In contrast, the Type C shows a slight increase in its two smallest size bins, and the sum over this "tail" (equal to ~ 2 μL/L) was the same magnitude as the sum of the smallest 6 bins of the Type-B. Although the LISST-Type C cannot resolve specifically size very small particles, this does suggest that in terms of total volume concentration integrated from 2.5 to 500 microns over the LISST-100 Type C likely do include an appropriate contribution from the < 2.5 micron particles in suspension. The relatively turbid water of the York River estuary implies that ambient light contamination is probably not a significant issue.

3.1.3 Total Suspended Solids and Organic Content:

Water samples collected by the CHSD profiler's high-speed pump were analyzed for TSS and organic content via standard gravimetric analysis combined with loss on ignition (USEPA, 1979 Methods No. 160). Pumped samples were placed in 1-liter dark plastic bottles, stored in an ice chest on deck, and filtered immediately upon returning to VIMS (no less than 8 hours later). Vacuum filtering was employed utilizing pre-weighed, 0.7 micron, 47-mm diameter glass fiber filters. After filtration, filters were rinsed with deionized water (using at least 1000 mL) to remove salt and were then oven-dried at 103-105°C for at least 24 hours. Filters were re-weighed and re-dried repeatedly until consecutive weights agreed to within 0.5 mg. The filters were then placed in a 540°C

oven for at least an hour, allowed to cool, and re-weighed to determine relative organic content via loss on ignition.

3.1.4 Water Density and viscosity

Water properties (density, viscosity, and depth) were determined from measurements of conductivity, temperature, and pressure collected by a YSI6600 Sonde CTD. On the profiler frame, the CTD samples at approximately the same height as the LISST-100X.

3.2 Analysis

3.2.1 Merging LISST-100X and PICS particle size distributions (PSDs)

The independent PSDs measured by the LISST-100X and PICS were merged to capture a larger size range of particles, 2.5-1000 microns. Others have successfully merged LISST-100X and camera-based observations of floc size and volume concentration in similar coastal and estuarine environments in order to increase PSD range and quality of floc-dominated PSDs (Mikkelsen et al., 2005, 2006; Hill et al., 2011). The LISST-100X was mounted on the profiling frame with its sampling window close enough to the PICS to assume the two instruments were sampling near-surface floc populations with similar statistical properties (Figure 2).

PICS and LISST-100X PSDs were merged following the methodology similar to that introduced by Mikkelsen et al., 2005. Particle volumes measured by the PICS were binned into 23 logarithmically spaced size bins from 30-1000 microns. The size bins were chosen to match and extend the size bins used by the LISST-100X. The instruments overlap from ~30 to 500 microns (16 size class bins). The standard output for the LISST-100X is in units of particle volume per sampling volume, μL/L, and is based on the manufacturer's provided, instrument-specific volume calibration constant (Agrawal and Pottsmith, 2000). The PICS sampling volume is considerably smaller than the LISST-100X's, and the volume captured in a given size class *i* by the PICS (V_{PICSi}) is limited to those particles which passed criteria for consistent size and shape across multiple video

frames. Therefore V_{PICSi} is generally much lower than LISST volume concentration (VC_{LISSTi}) and is more of a relative measure in units of particle volume (mm^3). The LISST-100X was chosen as the reference instrument, and V_{PICSi} was multiplied by a scaling factor (α) to estimate the equivalent PICS particle volume per sample volume, VC_{PICSi} in µL/L, if the PICS had measured the same sample volume as the LISST-100X. This approach assumes that the shape of the PICS distribution behaves conservatively over a range of sample volumes. α was determined for each sample by calculating the average ratio of LISST-100X volume concentration to PICS volume over a set range of *n* overlap bins *i:i+n*:

$$\alpha = \frac{\overline{VC_{LISST_{i:i+n}}}}{V_{PICS_{i:i+n}}} \qquad \text{Eqn. 3b.}$$

The range of the overlap bins (*i:i+n)* was determined individually for each sample. Multiple overlap regions were evaluated over the range of optical agreement (~70-300 µm) identified in previous analysis comparing the LISST-100X and PICS (Smith and Friedrichs, 2011). Cumulative volume statistics, d_{25}, d_{50} and d_{75} where, d_n indicates the *n* percent of the distributions volume is less than size d, were calculated using the volume distribution in only the size classes within the overlap range being assessed and compared (Figure 3, Mikkelsen et al., 2005). The overlap range with the strongest agreement between the two instruments was used to calculate α. The volume in all 23 of the PICS bins was multiplied by α to calculate the volume concentration (VC_{PICS}) in units of µL/L. Finally, the PICS and LISST-100X distributions were merged in the following manner (Figure CB): for bin size classes with lower limits of i=1.90 µm- lower value of overlap region, VC_i was assumed equal to VC_{LISSTi}; and for i=upper value of overlap region -1000 microns, VC_i was assumed equal to VC_{PICSi}. Within the overlap region, VC_i was set equal to the average of VC_{LISSTi} and VC_{PICSi}.

3.2.2 Fractal floc properties

Primary particle density (ρ_p) and size (d_p) were determined by combining video derived fractal properties, merged PSDs, and pump sampling. Fractal models and fractal dimension, F, were determined by best-fit power law functions fit to PICS measured Δρ

and d_f (Kranenburg 1994; Winterwerp 2002). Mass concentrations (TSS_p) were estimated from merged PSDs and PICS fractal models (Eqns. 2f,g) for a range of values of ρ_p, 100:1:3000 kg/m^3. Best-fit ρ_p was determined by matching fractal TSS_p to the observed mass concentration from pump samples (TSS). Specifically, ρ_p was defined as the density that produced the minimum difference between TSS_p and TSS. Primary particle size (d_p) was calculated from Eqn. 2d.

Pump samples were used to calculate an additional estimate of ρ_p, denoted as ρ_{tss}, using the fraction of inorganic ($F_{inororg}$) and organic material (F_{org}) determined via LOI and the respective densities (ρ_{org} and ρ_{inorg}):

$$\rho_{tss} = \frac{M_T}{V_T} = \frac{M_{inorg}+M_{org}}{V_{norg}+V_{org}} = \left[\frac{F_{inorg}}{\rho_{inorg}} + \frac{F_{org}}{\rho_{org}}\right]^{-1} \quad \text{Eqn. 3c}$$

(similar to Markussen and Anderson, 2013).

Eqn. 3e assumes uniform composition of F_{inorg}, F_{org}, and thus ρ_{tss} in a suspension. For simplicity, in the Eqn 3e the density of organic and inorganic solids, ρ_{org} and ρ_{inorg}, were defined as constants, where ρ_{inorg} = 2700 kg/m^3 and ρ_{org} = 1000 kg/m^3, chosen based on those suggested in the literature.

4. Results

4.1 Floc size (d_f) and fractal properties inferred from PSD and pump samples

Results reported here are from 65 distinct samples collected within the top 2-3 m of the water column, over a variety of hydrodynamic and meteorological conditions (i.e. spring neap, flood, ebb, high and low river flow, etc.). Total suspended solids mass concentrations (TSS) ranged from 10-100 mgL^{-1}. For more than 50% of the samples TSS was less than 25 mgL^{-1}. Bulk organic fraction of the TSS (F_{org}) ranged from 0.1-0.5, and was inversely related to TSS, such that as TSS increased F_{org} decreased (Figure 4A). Primary particle density inferred from TSS and F_{org} using Eqn. 3e, ρ_{tss}, ranged from 1515 kg/m^3- 2209 kg/m^3. Values are lower than that of pure clay minerals and higher than purely organic material, but are consistent with the hypothesis that primary particles are

not simply clusters of clay minerals, but rather exist as small aggregates composed of both inorganic minerals and less dense organic material (Fettweiss, 2008; Braithwaite et al., 2010; Maggi et al., 2013; Markussen and Anderson, 2013). Considering the composition of sediments and nature of organic matter for the York, ρ_{tss} inferred from TSS and F_{org} were realistic. Analysis of bed samples found that the inorganic material in the system is predominately Illite clays (~75%), with some contributions (~8%) of Kaolinite, Chlorite, and Smectite (Maa et al., 2002). The densities of these materials range from 2300-2800 kg/m^3 and the average density of Illite ~ 2750 kgm^{-3} (Tyson, 1995; Mehta, 2013). Typical particulate organic matter in the middle and lower York is derived from autochthonous sources, predominately zooplankton, phytoplankton, and bacteria, while the upper York particulate organic matter is more terrigenous, originating from higher order marsh plants, non diatom algal sources, and some freshwater zooplankton and phytoplankton (McCallister et al., 2006; Countway et al., 2007). The organic compounds associated with these sources (i.e proteins, lipids, amino acids, TEP etc.) span a range of densities from roughly 700-1600 kg/m^3 (Tyson, 1995; Malpezzi et al., 2013; Maggi and Tang, 2015).

LISST/PICS merged PSDs revealed the majority of the volume in suspension (approximately 80%) was attributed to particles less than 100 microns (Figure 4B). Overall, PSDs were fairly widely distributed over ≈2-300 microns. The median particle size by volume ($d50_v$) ranged from 20-90 microns, with an average of 48 +/- 20 microns. The average PSD of all samples is plotted as a solid black line in Figure 4B. It is characterized by a multimodal signal with peaks between 4-10 microns, 10-30 microns and around 100 microns. Following a four-level multimodal classification (Fettweis et al., 2012; Lee et al., 2012), PSDs suggest that suspensions in the York (by volume) are composed of microflocs, ≈50-200 microns, flocculi, ≈10-20 microns, and primary particles, >10 microns.

4.2 Fractal dimension (F) and floc excess density (Δρ) inferred from PICS

The PICS tracked over 150,000 individual particles. Sizes (d_f), settling velocities (w_s),

and excess densities ($\Delta\rho$) from all samples are presented in Figure 5. Over 80 percent of the particles tracked were between 40-100 microns. Results suggest a population of particles that do not settle (negative w_s, Figure 5A). Observations of negative w_s correspond to $\Delta\rho$ less than or equal to water, and represent the "washload" population of particles constantly in suspension (Cartwright et al, 2011; 2013).

There is observable scatter in the relationships between w_s, $\Delta\rho$ and d_f (Figure 5A,B). This is not unique or unexpected. Unlike noncohesive material, w_s and $\Delta\rho$ for flocs are not simply linearly correlated to d_f, but are influenced by the composition of their constituent particles (Winterwerp and Van Kesteren, 2006). The amount of scatter is similar to those observed in other environments with other video systems (Dyer and Manning, 1999; Khelifa and Hill, 2006; Fettweiss, 2008; Larsen et al., 2009; Maggi et al., 2013). In addition to the more complicated nature of settling of cohesive flocs, some of the noise is also associated with instrumentation. Despite using automated PIV analysis for improved estimates of the background fluid velocity (Smith and Friedrichs, 2015), there could still be some noise associated with PICS observations high in the water column, which would contribute to some scatter.

Scatter was accounted for by averaging w_s and $\Delta\rho$ over 75 logarithmically spaced particle size bins from 30-1000 microns. Bin-averaged w_s and $\Delta\rho$ (Figure 5C,D) suggest the presence of two fractal populations, microflocs and macroflocs, characterized by different fractal dimensions, F. A strong fractal relationship fits particles with d_f between ≈40-100 μm, $F_{40\text{-}100\ \mu m}$. A pronounced change in slope (i.e. kink) occurs between 100-200 microns, which suggests a second fractal population, $F_{>100\ \mu m}$, although the relationship is a bit noisier. "Kinks" have been noted before which has led to the idea that size varying fractal dimensions are more appropriate (Khelifa and Hill, 2006; Maggi et al., 2007).

Best-fit power law functions yield bulk fractal dimensions for the two populations (F_x). $F_{40\text{-}100\ \mu m}$ and $F_{>100\ \mu m}$ inferred from bin averaged w_s were 2.48 +/- 0.02 and 1.97 +/- 0.06 (Figure 5C), and from bin averaged $\Delta\rho$ were 2.53 +/- 0.02 and 2.04 +/- 0.1 (Figure 5D). $\Delta\rho$ is inferred from observed w_s (Eqn. 3a), so it is not surprising that the fractal approximations are similar. w_s results were merely shown as an example PICS observations. This study utilizes theory based on $\Delta\rho$, so for the remainder of the analysis

fractal relationships were determined solely from the relationship between bin-averaged $\Delta\rho$ and d_f. To ensure inferred fractal trends were not a result of bin-averaging, $\Delta\rho$ was also averaged over 50 and 100 size class bins. Fractal approximations were insensitive to the number of size class bins. Between the different means of averaging (50, 75 or 100 bins), estimates of $F_{40\text{-}100\ \mu m}$ and $F_{>100\ \mu m}$ varied from 2.52-2.56 and 2.04-2.14, respectively. The larger variability in $F_{>100\ \mu m}$ was expected due to low frequency of observations of particles at larger size classes. The average of $F_{40\text{-}100\ \mu m}$ and $F_{>100\ \mu m}$ inferred from PICS $\Delta\rho$ bin-averaged over 50, 75 and 100 bins was calculated and provided in Table 2.

The number of particles tracked by the PICS at each individual station ranged from ~40 to 8000. Naturally, the number of particles tracked by the PICS at each station was positively correlated to total suspended solids (Figure 4A). Because individual stations had considerably fewer particles, $\Delta\rho$ was bin averaged over 10, 20 and 30 size class bins. The lower number of tracked particles resulted in a bit more noise in bin-averaged $\Delta\rho$, especially at large sizes (Figure 7D). On average, only 10% of the particles tracked were larger than 100 microns, and less than 1% of particles were larger than 200 microns. For individual stations, we only attempted to identify only one fractal group, by fitting data from 40-100 microns, $F_{40\text{-}100\ \mu m.}$ Not all stations could be fitted with a realistic fractal model from PICS observations. A realistic $F_{40\text{-}100\ \mu m}$ was defined such that $1 < F_{40\text{-}100\ \mu m} < 3$ and that the standard deviation between bin sets (σ_F) was<0.2. 19 samples were flagged because realistic $F_{40\text{-}100\ \mu m}$ were could not able to be determined (Figure 4A). The max σ_F accepted was 0.16. $F_{40\text{-}100\ \mu m}$ ranged from 1.57-2.86, with an average $F_{40\text{-}100\ \mu m}$ of 2.36. PICS fractal dimensions are consistent to with fractal dimensions observed in other estuarine environments (Dyer and Manning, 1999; Sanford et al., 2005; Winterwerp and Van Kesteren, 2006; Smith and Friedrichs, 2011).

4.3 Inorganic Flocs vs. Organic Flocs

The observations in this study captured the well-documented gradient in total suspended solids and organic matter along the estuary (Figure 4A, Moore et al., 1997; Schaffner et al., 2001; Friedrichs et al., 2009). Unfortunately the majority of the samples that were not

able to be described with a fractal model were a lot of the more organic rich samples collected near the mouth. All these samples had fairly low suspended concentrations, so the PICS was unable to collect a lot of particle observations. In order to have enough particles to be able to use the PICS to examine the difference in fractal characteristics along this gradient, samples were pooled into two subsets that represent two characteristic end members of a typical partially mixed estuary, (1) Type 1: suspensions near the mouth, characterized by more organic rich but lower overall suspended sediment concentrations and (2) Type 2: suspensions near the ETM characterized high TSS and mostly inorganic suspended sediment concentrations. In our data, Type 1 suspensions were defined as samples that were in the upper 20% in terms of organic fraction (F_{org}>0.28) and lower 20% of TSS (TSS<20 mg/L). This group was made up of 16 samples total. Type 2 suspensions were defined as samples that were in the upper 20% of TSS (TSS> 40 $mg^{/L}$) and lower 20% of organic fraction (F_{org}<0.2), and contained a total of 5 samples.

Particle size distributions for Type 1 and Type 2 suspensions as well as the average of all samples are compared in Figure 6. Type 2 suspensions (blue) are fairly narrow and unimodal, with a peak around 100 microns; while Type 1 suspensions (red) are characterized by a wider and flatter distribution, with a slight peak <10 microns. Average d_{50v} is slightly higher for the Type 2 suspensions, d_{50v} =57 +/- 14 microns compared to d_{50v} =30 +/- 14 microns. A simple two-sample t-test found the difference in d_{50v} for the two to be significant with a p-value of 0.001. The results suggest the way organic matter influences floc size could be related to relative concentration of inorganic solids. The presence of organic matter has been observed to enhance floc growth when the concentration of inorganic solids is high (Sanford et al., 2005; Cross et al., 2013; Malpezzi et al., 2013; Fettweis et al., 2014). Type 1 suspensions are characterized by much lower inorganic sediment concentrations (<20 mg/L), so it lacks a source of material to create larger flocs. In terms of the multimodal classification, Type 1 suspensions contain a larger contribution of organic rich primary particles/flocculi, while Type 2 suspensions are predominately low organic microflocs.

Bin-averaged PICS observations of $\Delta\rho$ and d_f of Type 1 and Type 2 suspensions are

shown in Figure 7B,C. Each was binned over 50, 75 and 100 size class bins, and the results from 75 bins are shown. A pronounced change in slope (i.e. kink) was also resolved in these subsets between 100-200 microns and two fractal models were approximated (Table 2). $F_{40\text{-}100\ \mu m}$ was slightly higher, but not significantly, for Type 2 microflocs, 2.60 vs. 2.53. In both cases fewer larger flocs (d_f<100 microns) were tracked, so the value of $F_{>100\ \mu m}$ is not as well constrained as $F_{40\text{-}100\ \mu m}$. Nevertheless, there was a significant difference between $F_{>100\ \mu m}$ between Type 1 and Type 2 flocs, $F_{>100\ \mu m}$ =1.26, 2.34, respectfully. These results suggest that as particles become more organic, the change in F, from microflocs to macroflocs increases. This implies that larger organic flocs are less tightly packed than inorganic flocs of roughly same size. This has been has been documented before in other systems (Larsen et al., 2009; Maggi et al., 2013).

4.4 Theoretical relationship between excess density (Δρ) and apparent density (ρ_a): Application to field data

PICS fractal models and merged volume concentration particle size distributions (PSDs) were used to estimate ρ_p and d_p using the relationships between apparent density (ρ_a), excess density (Δρ), and fractal TSS (Eqn 3c, 3d; Ganju et al., 2007; Braihtwaite et al., 2010). Results were evaluated using the following quality control criteria:

(1) Best-fit primary aggregate density (ρ_p) was in a realistic range based on the observed range from F_{org}, $1200 < \rho_p < 2400$ (Eqn.3e). This range was determined by calculating ρ_p for the observed values of F_{org} over the range of possible ρ_{inorg} (2600-2800 kg/m^3) and ρ_{org} (700-1600 kg/m^3) for the York (Maa et al., 2002; Mehta, 2014; Tyson; 1994).

(2) Best fit primary particle aggregate size (d_p) were in realistic ranges suggested by the literature where $0.1 < d_p < 10$ μm (Winterwerp et al, 1998; Fettweis, 2008; Mehta, 2014).

(3) The density of organic matter calculated using estimated ρ_p, F_{org} and F_{inorg}, ρ_{org} (Eqn. 3e), was within in realistic ranges suggested by the literature $700 < \rho_{org} < 1600$ kg/m^3 for the system.

Application of the theoretical analysis to the data produced encouraging results. Results are shown on the bin-averaged plots in Figure 7 and in Table 2. The solid lines represent fractal approximations of $\Delta\rho$ (black) and ρ_a (red), where ρ_a was calculated using the best-fit ρ_p and Eqn. 3d. ρ_{tss}, and best-fit ρ_p and d_p are annotated in the bottom left corner of each figure. Best-fits were determined for F_x - σ_F, F_x, and F_x + σ_F. Standard errors for ρ_p and d_p were defined as the standard error around the mean of the values from F_x +/- σ_F. Standard errors for ρ_{tss} for the case containing all particles (Figure 7A), Type 1 (Figure 7B) and Type 2 (Figure 7C), are related to the range of F_{org} for the samples within these groups. Best-fit ρ_p for the surface waters of the York (i.e. all samples combined) was 1751 +/- 12 kg/m^3 and d_p was 1 +/- 0.1 microns. For organic (Type 1) flocs, best-fit $\rho_p \approx 1551 \pm 29$ kg/m^3 and $d_p \approx 1.4$ +/- 0.6. Inorganic (Type 2) flocs had higher best-fit $\rho_p \approx 2278 \pm 68$ kg/m^3 and lower $d_p \approx 0.6$ +/- 0.1 microns. For these three cases, best-fit ρ_p agreed quite well with ρ_{tss}, and best-fit d_p were within range of previously established values (Khelifa and Hill, 2006; Braithwaite et al., 2010; Fettweis, 2008; Chapalain et al., 2018). This suggests, at least in a bulk sense, that a simple fractal approximation based on two particle populations (microflocs and macroflocs) appropriately describes surface flocs in the York River estuary, and that as flocs became more organic, ρ_p decreases and d_p increases.

Analysis on individual stations was a bit more complicated, as video observations were a bit noisier, and contained much fewer flocs to negate noise. Based on the criteria listed above (1-3), fractal models were only "confidently" fit to 18 of 65 samples. An example of a station that was successful is shown in Figure 7D. Initially, 19 stations were disregarded because a realistic F_x could not be defined, while the remainder produced unrealistic values for ρ_p, d_p and/or ρ_{org}, However, for the 18 samples that fit the critera, best-fit ρ_p agreed notably well with corresponding observations ρ_{tss} (Figure 8A note the 1:1 line). On average the percent difference was ~7%. The largest difference observed was about 20% or ~ 320 kg/m^3. Considering the assumptions involved with ρ_{tss}, (1) ρ_{org}= 1000 kgm^{-3}, (2) ρ_{inorg}= 2700 kgm^{-3}, and (3) ρ_{org} and ρ_{inorg} are the same for all particles in suspension, a 20 % difference is not excessive. As an additional check, ρ_{tss} was calculated over the entire range of possible values suggested by the literature for ρ_{org} (700 kg/m^3< ρ_{org} < 1600 kg/m^3) and ρ_{inorg} (2300 kg/m^3< ρ_{org} < 2700 kg/m^3). All best-fit ρ_p were well within one standard error of the mean ρ_{tss} calculated for the different ranges. Best-fit d_p

ranged from 0.1-8.9 microns, with an average d_p of 3.2 microns (Figure 8B).

Table 2: Summary of fractal analysis results. Average results of 3 bin sets used (50, 75 and 100).

Group	TSS [mg/L]	OSS [mg/L]	F_{org}	ρ_{TSS} [kg/m^3]	$F_{40\text{-}100\ \mu m}$	$F_{>100\ \mu m}$	ρ_p [kg/m^3]	d_p [µm]
ALL	28 ± 19	6 ± 3	0.24	1884 ±141	2.53 ± 0.02	2.09 ± 0.06	1751 ± 12	1.0 ± 0.1
Type 1	14 ± 4	11 ± 2	0.32	1728 ± 105	2.60 ± 0.1	1.26 ± 0.1	1551 ± 29	1.6 ± 0.3
Type 2	68± 20	4 ± 1	0.17	2088 ±105	2.53 ± 0.03	2.34 ± 0.03	2267± 29	0.6 ± 0.1

4.5 Controls on Fractal Properties

Samples that were confidently described using a fractal model were used to investigate controls on ρ_p, d_p, and F, including organic fraction (F_{org}), total suspended solids concentration (TSS), salinity, and current velocity (U). Even though analysis is limited to a small number of samples, some trends are suggested. By definition (i.e. Eqn. 3e), $\rho_{tss} \alpha F_{org}$. Best-fit ρ_p (Figure 8A) and d_p (Figure 8B) were fairly well-correlated to ρ_{tss}, thus F_{org} (p-values ≈0.005 and 0.06). As fractal flocs become more organic, ρ_p decreased and d_p increased. This is consistent with the results of the comparison between Type 1 and Type 2 suspensions (Table 2) and the results of others who used the same (Chapalain et al., 2018) or similar fractal approach (Maggi et al., 2013; 2015) to estimate d_p. More direct measurements of d_p by Fettweis (2008) on samples collected in the southern North Sea using a Sedigraph 5100 found that d_p increased offshore where organic matter was higher.

There was not a clear relationship between F and ρ_{tss}, and the data was bit noisy (Figure 8C), which could be attributed sample size being limited to 18 points or the range of organic fraction we are considering, 0.1-0.4. F was somewhat correlated to d_p, p-value=0.01 (Figure 8D) and as d_p decreased, F decreased. Both Chaplain et al., 2018 and

Fettweis 2008 conclude that F was more strongly influenced by d_p than organic matter alone. Fettwies 2008 highlights the importance of constraining ρ_p and d_p when assuming a fractal model to approximate excess density, while Khelifa and Hill, 2006 stress the importance of the same primary particle properties to determine F. These results, though a bit sample limited, bring about a similar conclusion, emphasizing the importance of constraining ρ_p and d_p in the fractal approach.

The relationship between other parameters, TSS, salinity and U, but did not appear to influence fractal dimension or primary particle properties (Figure 9). Although, looking at the relationships between U and TSS, and median floc size by volume, d_{f50} (Figure 10), suggests that U influences floc characteristics. Observations suggest that higher U spreads higher concentrations of larger, lower organic content flocs up into surface waters, which affects floc size. Again these interpretations are limited to 18 samples, and are broad speculations. More observations are needed to better explain the relationships.

5. Discussion

5.1 Theoretical Characterization of primary particle density (ρ_p) and size (d_p)

We presented a method to characterize primary particle density (ρ_p) and size (d_p) and evaluate fractal approximations. It requires independent, co-located observations of particle size distributions, total suspended solids and organic fraction, and individual particle size (d_f) and corresponding $\Delta\rho$, ρ_a or settling velocity (w_s). The method was built upon the method introduced in Ganju et al., 2007 and Braithwaite et al., 2010. Previous applications automatically assumed fractal behavior and required somewhat subjective assumptions to constrain ρ_p and d_p. Braithwaite et al., 2010 constrained best-fit guesses by 1000 kg/m^3 $<\rho_p<$ 3000 kg/m^3, and 1 μm $<d_p<$ 10 μm, while Bowers et al., 2017 and Chaplain et al., 2018 assumed constant ρ_p and d_p. The studies yielded reasonable results for best-fit F and Braithwaite et al., 2010 concluded reasonable estimates of ρ_p and d_p. However, the constraints placed on F, ρ_p and d_p places an inherent bias on the results, because only reasonable values were evaluated as potential best-fit values. Additionally,

because resulting best-fit F, ρ_p and d_p are dependent of one another, none can be validated by another.

The method proposed here used realistic constraints to characterize fractal and primary particle properties, and incorporated easily obtainable and independent supporting measurement to validate the results. Rather than using optimization to characterize F, F was inferred from in situ measurements of floc $\Delta\rho$ and d_f collected using a high definition particle settling camera (PICS). This way, no initial fractal assumptions were made. Observations were used to identify whether suspensions demonstrate fractal behavior and then characterize representative fractal relationships (F) when appropriate. With independent observations of F, solutions are only needed for two unknowns (ρ_p and d_p) and PICS derived F provides a realistic constraint on the optimization for ρ_p and d_p. Second, an independent measurement of bulk primary particle densities (ρ_{TSS}) was inferred from the organic fraction of the total suspended solids of the pump samples. The consistency between fractal ρ_p and ρ_{TSS} was used to check the validity on the fractal model, and thus best-fit ρ_p and d_p. Regardless of whether independent estimates of F are available, ρ_{TSS} is useful in constraining best-fit ρ_p, and could provide constraints to optimization of F and d_p.

This novel approach was applied to samples collected throughout the surface waters of the York River estuary. Samples were collected during three different years, during variety of hydrodynamic and meteorological conditions, throughout the system. In doing so, the samples exhibited a range of total suspended solid concentrations (~order of magnitude, 10-100 mg/L) and organic content (10%-50%). For most samples, a simple fractal relationship described by a constant fractal dimension was defined. For pooled samples there were enough observations of larger flocs to distinguish and characterize two fractal groups, but models were still relatively simple. Despite the simplicity of the fractal models, estimates of ρ_p were remarkably consistent with ρ_{TSS}. Results suggest that over a variety of sediment and hydrodynamic conditions, simple fractal models derived from video settling relationships, can be used to accurately describe surface populations and used to characterize primary particle characteristics.

5.2 Implications for Fractal Models

Understanding the controls on floc settling velocity and density in coastal environments is crucial. Flocculated sediments reduce light availability for primary producers, promote the transport of toxic materials or nutrients throughout the system, influence the delivery of sediment to bed directly impacts navigational channels or macrobenthic environments (Reay, 2009; Bowers et al., 2011; Smith and Friedrichs, 2011; Law et al., 2014). Many mathematical models have been developed to evaluate floc dynamics in coastal systems. These models range in complexity from a basic power-law function relating settling velocity or density to size (Kranenburg, 1994; Winterwerp, 1998; Khelifa and Hill, 2006), to a simple single population models that investigate change in floc diameter over time (Winterwerp, 2002; Son and Hsu, 2011), to slightly more complex two-class population models can resolve bimodal flocculation (Lee et al., 2014), to the most sophisticated multi-class models (Maggi et al., 2007; Verney et al., 2011). The different models vary in complexity and ability, but all of them assume a fractal approach and require input of fractal dimension, primary particle size, and density. It is common to set primary particle density near that of quartz or clay and size as 1,4, or 10 microns (Winterwerp et al., 1998; Manning and Dyer, 1999; Sanford et al., 2005; Son and Hsu, 2011; Verney et al., 2011; Hurley et al., 2016). These parameters also can be treated as adjustable fitting parameters (Lee et al., 2014). Fractal dimension is either assumed to be constant (Winterwerp et al., 1998; Son and Hsu, 2011; Vernay et al., 2011) or vary with size (Maggi et al., 2013; Son and Hsu; 2011; Vernay et al., 2012). Son and Hsu, 2011 compared simulations that used a constant fractal dimension to simulations using size-varying fractal dimensions, and found the size varying fractal dimension better captured essential feathers of cohesive sediment transport in the Ems/Dollar estuary. Verney et al., 2011 also compared fractal dimension assumptions, as well as the influence of primary particle size, and found that small variability in fractal dimension did not have nearly as significant of an effect on the results, as changes in the primary particle size. The importance of primary particle size and density is also suggested in Khelifa and Hill, 2006 and Fettweis, 2008. Both note that the main uncertainties in fractal approximations of floc density and settling velocity are associated with the characterization of primary

particle size and density. The work here presents a method to characterize primary particle density (ρ_p) and size (d_p). This approach is a valuable technique to quantify these hard to constrain, but extremely important fractal parameters that will improve floc models.

Another major advantage of this approach is its potential to validate proposed fractal models. Fractal theory requires $1 \leq F \leq 3$ (Kranenburg, 1994). Generally, estimates of F are accepted as long as values are within the appropriate range and appear to fit the data graphically (Khelifa and Hill, 2006). This approach introduces the concept of using an independent measurement of bulk primary particle densities inferred from totals suspended solid samples (ρ_{tss}) to validate F. The approach was evaluated for samples collected in the York River estuary with a PICS system, but is quite applicable in other environments and has the potential to provide huge insights into the fractal nature of flocs in coastal and estuarine systems. The key requirement is that fractal models must be from a source independent of the PSDs and observed TSS.

5.3 Uncertainties

Although the results offered great insight into fractal approximations derived from settling relationships, they also raise some important questions regarding the approach and the fractal nature of surface flocs. For instance, in a bulk sense (cases where multiple samples were grouped) suspensions were well described by fractal models, but when applied to individual stations, only 18 stations were confidently described using the PICS derived fractal model. For the samples in which confidence criteria was not met, is this attributed to systematic limitations associated with the PICS and the LISST-100X? Are the fractal assumptions too simple? Are fractal approximations the best way to describe surface flocs, which are a mixture of organic and inorganic solids, rather than dominantly inorganic? These questions are examined in the remainder of the discussion.

5.3.1 PICS Fractal Model

It is important to consider the systematic limitations of the PICS that will influence the observations of floc size and excess density, and resultant fractal models, specifically limitations at smaller particle sizes and low mass concentrations. Small flocs (d_f<100 microns) made up a significant contribution of surface suspensions (Figure 4B, 5), and at most stations had suspended solid concentrations were less than 25 mg/L (Figure 4A). Both limit the number of particles available for the PICS to successfully track. Recall the fraction of the total number of particles present that are successfully tracked is reduced at smaller sizes relative to larger sizes (Sec. 3.1.1). In addition, post-analysis revealed that the laser intensity or lighting illumination setting used to collect these samples was less than ideal. The poor illumination made it that much more difficult to identify and track smaller flocs, even for those within the PICS resolution range. Despite PIV analysis, the nature of flocs still results in a bit of scatter the observations. An appropriate fractal model may not have been determined because the suspensions were not fully resolved or not enough observations were available to average out the noise. Significantly fewer particles were tracked when considering individual stations compared to pooled cases (~100s vs 10,000s). Pooled samples contain enough observations throughout the smaller end of the resolution range (30 microns <d_f<100 microns), that limitations were not overwhelming.

5.3.2 Consistency Between Pump samples and PSDs

We also consider whether estimates of total suspended solids (TSS) from PSDs and TSS observed from pump samples were based on compatible particle size ranges. If the size range of particles contributing to TSS is greater than the range contributing to ΣVC_i, ρ_a will be overestimated (Bowers et al., 2009). Overestimating ρ_a, underestimates ρ_p (Eqn. 2c) and overestimates d_p (Eqn. 2e). The nominal pore size of the glass fiber filters used here is 0.7 μm, so all particles larger than this can be caught on the filter and contribute to TSS. Merging the PICS and LISST extends the size range of VC_i up to 1000 microns. All PSDs dropped off sharply well before 1000 microns (Figure 4B) and very few large flocs were identified by the PICS (less than 1% with d_f>200 microns). Data suggests that particles with diameters larger than the combined PSD range did not contribute

significantly to TSS. As for particles smaller than the LISST-100 Type C resolvable range (d_f<2.5 mircons), simultaneous sampling with a co-located LISST-100x Type B (range 1.25-250 microns), determined that although the LISST was not resolving particles smaller than 2.5 microns, total volume concentration integrated from 2.5 to 500 microns still includes an appropriate contribution from the < 2.5 micron particles in suspension. It is believed that the size ranges were compatible and were not a major source of error.

5.3.3 Fractal Assumptions

Finally, we consider the assumptions regarding fractal and primary particle characteristics. The method assumed very simple fractal models could represent an entire suspension. On top of this, the fractal dimensions were defined using a subset of sizes in suspension, 40-100 microns and >100 microns, when enough observations were available. Comparison between LISST-100X size distributions and PICS size distributions showed strong agreement between over ~60-250 microns (this study and Smith and Friedrichs, 2011). Additionally, over 80 percent of the particles tracked were between 40-100 microns. The fractal fit range includes the dominant sizes in suspension, as well as the sizes we have the most confidence in the PICS measuring. Despite the reasons, the assumption of one fractal dimension may still be too simple.

It is important to keep in mind, fractal approximation is an idealized way to describe flocs, Due to large variability of properties such as mineral composition, particle size distribution and organic-matter content, it is unlikely that flocs are truly self-similar structure, and can be simple described by one fractal dimension. In order to use the relationship between excess and apparent density (Eqn. 2e), without independent measurements of both, it was necessary to assume all flocs in suspension were composed primary particles that were uniform and in size and composition (i.e. density). Primary particle densities inferred from the bulk organic fraction in the pump samples are also constrained by the same assumption.

It is becoming popular to assume a fractal dimension that varies with floc size (Khelifa and Hill, 2006; Maggi et al., 2007; Kumar et al., 2010; Maggi et al., 2013). The slight curve observed in the log-log plots of d_f and $\Delta\rho$ (Figure 7), support the idea of a size varying fractal dimensions. To investigate if a more complex, varying fractal dimension was appropriate, a size varying F was derived using Khelifa and Hill, 2006 model. Three simulations were considered (1) using inputs for primary particle size, density, characteristic floc size and fractal dimension from Khelifa and Hill, 2006, d_p=1 micron, ρ_p =2300 kg/m^3, d_{fc}=2 mm, F_{dc}=2 (2) using PICS observations to define the characteristic floc size and fractal dimension and fitting PSDs to TSS to estimate ρ_p and d_p (3) using PICS observations and ρ_{tss} from pump samples and fitting PSDS to TSS to determine d_p. For cases (2) and (3) characteristic floc size was assumed to be 80 microns (size class with the most observations that the PICS tracks well) and the PICS derived $F_{40\text{-}100\mu m}$ was defined as the characteristic fractal dimension. None of the approaches were successful. For the base case (1), both predicted TSS and $\Delta\rho$ were overestimated $\Delta\rho$. For (2) and (3), $\Delta\rho$ was underestimated and the best-fit ρ_p was unrealistically low (<1100 kg/m^3). In fact, only 1 station in (2), produced results that would be acceptable according to the established criteria in this study. These results suggest that simple approximations describe the observations just as well (if not better) than more complex fractal dimensions when a characteristic floc size and dimension, primary particle size and density, are not well constrained. It also supports the idea that fractal assumptions may not be as easily applicable for surface suspensions.

Finally, we must consider that near surface flocs may not be able to be characterized as one fractal population. Particles in the surface water in estuarine and coastal environments are affected by irregular advection events (Fugate and Friedrichs, 2003), and also tend to contain a relatively larger fraction of organic matter. This potentially is introducing different fractal and non-fractal populations to a given suspension. For the York stations specifically, small resilient mud fecal pellets, that have been documented to influence near bed settling velocities (Cartwright et al., 2011; Fall et al., 2014) were observed to be quite dominant in some of the surface samples that could not be fit with a fractal model.

6. Conclusions

This paper presented a method to characterize primary particle density (ρ_p) and size (d_p) and evaluate fractal approximations. This novel approach was successfully applied to observations of near-surface particle properties collected in the York River estuary. Results yield fresh insights on fractal properties of near surface estuarine particles, as well as important implications for fractal approximations and advice for investigating fractal characteristics:

- Flocs are very hard to measure in-situ. Proper lighting and careful sampling is extremely important (especially in surface waters), where concentrations are low, particles are small and tend to be more organic.
- The relationship between excess and apparent density is a good way to evaluate the validity of fractal descriptions.
- Fractal approximations may not always hold high in the water column. Perhaps it is different near the bed or in cases when inorganic flocs dominant suspensions.
- Organic matter is the dominant influence on fractal properties.
- Fractal dimension does not appear to be as important to constrain in fractal approximation, as primary particle size and density.
- Using a more complicated size-varying fractal dimensions (Khelifa and Hill, 2006) did not describe suspensions any better then a simple approach.

7. References

Agrawal, Y.C., Pottsmith, H.C., 2000. Instruments for particle size and settling velocity observations in sediment transport. Marine Geology 168: 89-114.

Agrawal, Y.C., Whitmire, A., Mikkelsen, O.A., Pottsmith, H.C., 2008. Light scattering by random shaped particles and consequences on measuring suspended sediments by laser diffraction. Journal of Geophysical Research, Vol. 113. doi: 10.1029/2007JC004403.

Andrews, S., Nover, D., Schladow, S.G., 2010. Using laser diffraction data to obtain accurate particle size distributions: the role of particle composition. Limnology and Oceanography: Methods 8, 507-526.

Bowers, D.G., Braithwaite, K.M., Nimmo-Smith, W.A.M., Graham, G.W., 2009. Light scattering by particles suspended in the sea: The role of particle size and density. Continental Shelf Research, 29, 1748-1755.

Bowers, D.G., Braithwaite, K.,M., Nimmo-Smith, W.A.M., Graham, G.W., 2011. The optical efficiency of flocs in shelf seas and estuaries. Estuarine, Coastal, and Shelf Science 91: 31-350.

Bowers DG, McKee D, Jago CF, Nimmo-Smith W.A.M., 2017. The area to-mass ratio and fractal dimension of marine flocs. Estuarune, Coastal and Shelf Science 189:224–234. https://doi.org/10.1016/j.ecss.2017.03.026

Braithwaite, K.M., Bowers, D.G., Nimmo Smith, W.A.M., Graham, G.W., Agrawal, Y.C., Mikkelsen, O.A., 2010. Observations of particle density and scattering in the Tamar Estuary. Marine Geology, 277, 1-10.

Cartwright, G.M., Friedrichs, C.T., Sanford, L.P., 2011. In situ characterization of estuarine suspended sediment in the presence of muddy flocs and pellets. In: N.C. Kraus and J J.D. Rosati (eds.), Coastal Sediments 2011, American Society of Civil Engineers, 14 p.

Cartwright, G.M., Friedrichs, C.T., Smith, S.J., 2013. A test of the ADV-based Reynolds-flux method for in situ estimation of sediment settling velocity in a muddy estuary. Geo-Marine Letters, 33: 477-484. doi:10.1007/s00367-013-0340-4

Chapalain, M., Verney, R., Fettweis, M. & Jacquet, M., Le Berre, D., Hir, P., 2019. Investigating suspended particulate matter in coastal waters using the fractal theory. Ocean Dynamics. 69. 59-81. 10.1007/s10236-018-1229-6.

Countway, R.E., Canuel, E.A., Dickhut, R.M., 2007. Sources of particulate organic matter in surface waters of the York River, VA estuary. Organic Geochemistry 38. 365-279.

Cross, J., Nimmo-Smith, W.A.M., Torres, R., Hosegood, P.J., 2013. Biological controls on resuspension and the relationship between particle size and the Kolmogorov length

scale in a shallow coastal sea, Marine Geology 343, 29-38.

Dyer, K.R., Manning, A.J., 1999. Observation of the size, settling velocity and effective denisity of flocs, and their fractal dimensions. Journal of Sea Research. 41: 87-95.

Fall, K.A., Harris, C.K., Friedrichs, C.T., Rinehimer, J.P., Sherwood, C.R., 2014. Model behavior and sensitivity in an application of the cohesive bed component of the Community Sediment Transport Modeling System for the York River Estuary, VA. Journal of Marine Science and Engineering, 2(2): 413-436; doi: 10.3390/jmse2020413.

Fennessy, M.J., Dyer, K.R., Floc population characteristics measured with INSSEV during the Elbe Estuary intercalibration experiment. Journal of Sea Research 26, 55-62.

Fettweis, M., 2008. Uncertainty of excess density and settling velocity of mud flocs derived from in situ measurments. Estuarine, Coastal and Shelf Science, 78, 426-436

Fettweis, M., Baeye, M., Lee, B. J., Chen, P., & Jason, C. S., 2012. Hydro-meteorological influences and multimodal suspended particle size distributions in the Belgian nearshore area (southern North Sea). Geo-Marine Letters, 32(2), 123-137.

Fettweis, M., Baeye, M., 2015. Seasonal variation in concentration, size, and settling velocity of muddy marine flocs in the benthic boundary layer. Journal of Geophysical Research: Oceans 120, 5648-5667, doi:10.1002/2014JC010644.

Friedrichs, C.T, Cartwright, G.M., Dickhudt, P.J., 2008. Quantifying benthic exchange of fine sediment via continuous, noninvasive, measurements of settling velocity and bed erodibility, Oceanography: Special issue on coastal ocean processes observing technologies and models. Vol. 21, No. 4.

Friedrichs, C.T., 2009. York River physical oceanography and sediment transport. Journal of Coastal Research: Special Issue 57 – The Chesapeake Bay NERRS in Virginia: A Profile of the York River Ecosystem [Moore & Reay]: pp 17-22.

Fugate, D.C., Friedrichs, C.T., 2003. Controls on suspended aggregate size in partially mixed estuaries. Estuarine, Coastal, and Shelf Science. 58:389-404

Ganju, N.K., Schoellhamer, D.H., Murrell, M.C., Gartner, J.W., Wright, S.A., 2007. Constancy of the relation between floc size and density in San Francisco Bay. In: Maa, J.P.-Y., Sanford, L.P., Schoellhamer, D.H. (Eds.), Estuarine and Coastal Fine Sediments Dynamics. Elsevier Science B.V., Amsterdam, pp. 75–91.

Hill, P.S., Boss, E., Newgard, J.P., Law, B.A., Milligan, T.G., 2011. Observations of the sensitivity of beam attenuation to particle size in a coastal bottom boundary layer. Journal of Geophysical Research, Vol 116, doi: 10.1029/2010JC006539.

Hill, P. S., Bowers, D. G., & Braithwaite, K. M., 2013. The effect of suspended particle compositionon particle area-to-mass ratios in coastal waters. Methods in Oceanography, 7, 95-109.

Hurley A.J., Hill., P.S., Milligan, T.G., Law, B.A., 2016. Optical methods for estimating apparent density for sediment in suspension. Methods in Oceanography 17, 15-168.

Khelifa, A., Hill, P.S., 2006. Models for effective density and settling velocity of flocs. IAHR Journal of Hydraulic Research 44, 390-401.

Kumar, G.R., Strom, K.B., Kyvani, A., 2010. Floc properties and settling velocity of San Jacinto estuary mud under variable shear and salinity conditions. Continental Shelf Research 30, 2067-2081.

Kranenburg, C., 1994. The Fractal Structure of Cohesive Sediment Aggregates. Estuarine, Coastal, and Shelf Science 29, 451-460.

Larsen, L.G., Harvey, J.W., Crimaldi, J.P., 2009. Morphologic and transport properties of natural organic floc. Water Resources Research, Vol. 45, W01410, doi:10.1029/2008WR006990.

Lee, B.J., Fettweis, M., Tooman, E., Molz., F.J., Multimoldality of particle size distribution of cohesive particle matters in a coastal zone. Journal of Geophysical Research., Vol 117, C03014, doi:10.1029/2011JC007552.

Lee, B.J., Toorman, E., Fettweis, M., 2014. Multimodal particle size distributions of fine-grained sediments: mathematical modeling and field investigation. Ocean Dynamics 64, 429-441, doi: 10.1007/s10236-014-0692-y

Lintern, G., and Sills, G., 2006. Techniques for automated measurement of floc properties. J. Sediment. Res. 76:
1183–1195. doi:10.2110/jsr.2006.085

Maa, J.P.Y., Kim, S.C., 2002. A constant erosion rate for fine sediment in the York River, Virginia. Environmental Fluid Mechanics 1: 345-360.

Maggi F., 2007. Variable fractal dimension: a major control for floc structure and flocculation kinematics of suspended cohesive sediment. J Geophys Res Oceans 112. https://doi.org/10.1029/2006JC003951

Maggi F., 2013. The settling velocity of mineral, biomineral, and biological particles and aggregates in water. J Geophys Res Oceans 118:2118–2132.
https://doi.org/10.1002/jgrc.20086

Maggi F., Tang F.H.M., 2015. Analysis of the effect of organic matter content on the architecture and sinking of sediment aggregates.Mar Geol 363:102–111.
https://doi.org/10.1016/j.margeo.2015.01.017

Markussen T.N., Andersen T.J., 2013. A simple method for calculating insitu floc settling velocities based on effective density functions.Mar. Geol 344:10–18.
https://doi.org/10.1016/j.margeo.2013.07.002

McCallister, S.L., Bauer, J.E., Ducklow, H.W., Canuel, E.A., 2006. Sources of estuarine

dissolved and particulate organic matter: A multi-tracer approach. Organic Geochemistry 37, 454-468.

Mehta A.J., 2013. *An Introduction to Hydraulics of Fine Sediment Transport*. Advanced Series on Ocean Engineering, 38. World Scientific Publishing Co., Singapore.

Mikkelsen O.A., Pejrup, M., 2001. The use of a LISST-100 in-situ laser particle sizer for in situ estimates of floc size, density and settling velocity. Geo-Marine Letters, 20, 187–195

Mikkelsen, O. A., Milligan, T. G., Hill P.S., Moffatt, D., 2004. INSSECT—an instrumented platform for investigating
floc properties close to the seabed. Limnol. Oceanogr. Methods. 2: 226–236. doi:10.4319/lom.2004.2.226

Mikkelsen O.A., Hill P.S., Milligan T.G., Chant R.J., 2005. In situ particle size distributions and volume concentrations froma LISST-100 laserparticle sizer and a digital floc camera. Cont Shelf Res 25:1959–1978. https://doi.org/10.1016/j.csr.2005.07.001

Mikkelsen O.A., Hill P.S., Milligan T.G., 2006. Single-grain, microfloc and macrofloc volume variations observed with a LISST-100 and a digital floc camera. J Sea Res 55:87–102. https://doi.org/10.1016/j.seares.2005.09.003

Milligan, T. G., Hill, P.S., 1998. A laboratory assessment of the relative importance of turbulence, particle composition, and concentration in limiting maximal floc size and settling behaviour. J. Sea Res. 39: 227–241. doi:10.1016/S1385-1101(97)00062-2

Moore, K.A., Wetzel R.L., and Orth, R.J., 1997. Seasonal pulses of turbidity and their relations to eelgrass (Zostera marina L.) survival in an estuary. Journal of Experimental Marine Biology and Ecology, 215(1), 115-134.

Ostu, N., 1979. A threshold selection method from gray-level histogram, *IEEE Trans. Syst. Man Cybern.*, vol. 9, pp. 62-66.

Reay W., 2009. Water quality within the York River Estuary. Journal of Coastal Research. SI 57: 23-39

Sanford, L.P., Dickhudt, P.J., Rubiano-Gomez, L., Yates, M., Suttles, S.E., Friedrichs, C.T., Fugate, D.D., Romine, H., 2005. Variability of suspended particle concentrations, sizes, and settling velocities in the Chesapeake Bay turbidity maximum. In: Droppo, I.G., Leppard, G.G., Liss, S.N., Milligan, T.G. (Eds.), Flocculation in Natural and Engineered Environmental Systems.

Schaffner, L.C., Hinchey, E.K., Dellapenna, T.M., Friedrichs, C.T., Neubauer, M.E., Smith, M.E., Kuehl, S.A., 2001. Physical energy regimes, sea-bed dynamics and organism- sediment interactions along an estuarine gradient. In: Aller, J.Y., Woodin,

S.A., Aller, R.C. (Eds.), Organism–sediment Interactions. University of South Carolina Press, Columbia, SC, pp. 159–179.

Sin, Y., Wetzel, R.L., Anderson, I.C., 1999. Spatial and temporal characteristics of nutrient and phytoplankton dynamics in the York River Estuary, Virginia: Analyses of long-term data. Estuarines and Coasts, Volume 22, Issue 2, pp 260-275.

Smith S.J., Friedrichs C.T., 2011. Size and settling velocities of cohesive flocs and suspended sediment aggregates in a trailing suction hopper dredge plume. Continental Shelf Research 31,S50–S63.

Smith, S. J., Friedrichs, C.T., 2015. Image processing methods for in situ estimations of cohesive sediment floc size, settling velocity, and density. Limnology and Oceanography Methods, in press (downloadable at http://www.vims.edu/~cfried/cv/)

Soulsby, R. L. 1997. Dynamics of marine sands. Thomas Telford.

Tyson, R., 1995. Sedimentary organic matter : Organic facies and palynofacies / R.V. Tyson. (1st ed.). London ; New York: Chapman & Hall.

USEPA, 1983. Methods fro Chemical Analysis of Water and Wastes. Methods No. 160

Verney R, Lafite R, Claude Brun-Cottan J, Le Hir P (2011) Behaviour of a floc population during a tidal cycle: laboratory experiments andnumerical modelling. Cont Shelf Res 31:S64–S83. https://doi.org/10.1016/j.csr.2010.02.005

Winterwerp, J.C., 1998. A simple model for turbulence induced flocculation of cohesive sediment. Journal of Hydraulic Research, 36(3): 309-326. doi: 10.1080/00221689809498621.

Winterwerp, J.C., 2002. On the flocculation and settling velocity of estuarine mud. Continental Shelf Res., 22: 1339-1360.

Winterwerp, J.C., van Kesteren, W.G.M., 2004. Introduction to the Physics of Cohesive Sediment in the Marine Environment, Developments in Sedimentology series, 56. Elsevier, Amsterdam.

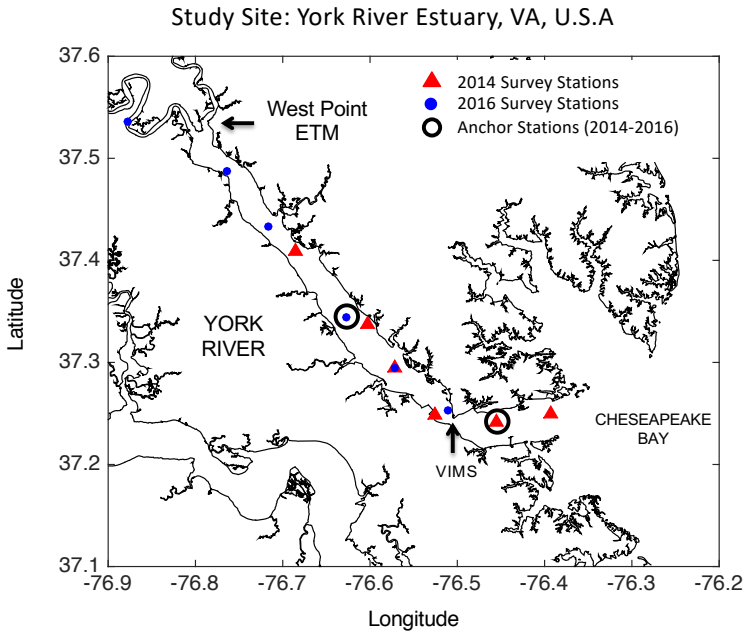

Figure 1: Map of the York River estuary, southeastern Virginia. Profiler Survey locations are indicated by the red triangles (2014) and blue circles (2016). Anchor station locations are circled in black (2014-2016).

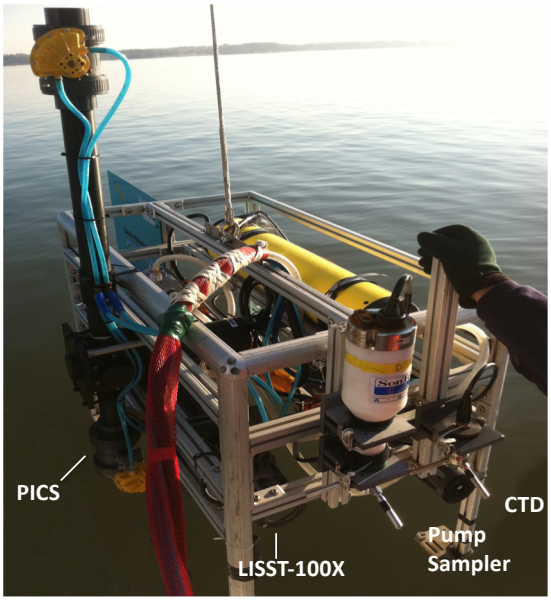

Figure 2: Photo of the Coastal Hydrodynamics & Sediment Dynamics (CHSD) water column profiler indicating the position of the pump sampler, PICS, LISST-100X and CTD. *Courtesy of G. Cartwright.*

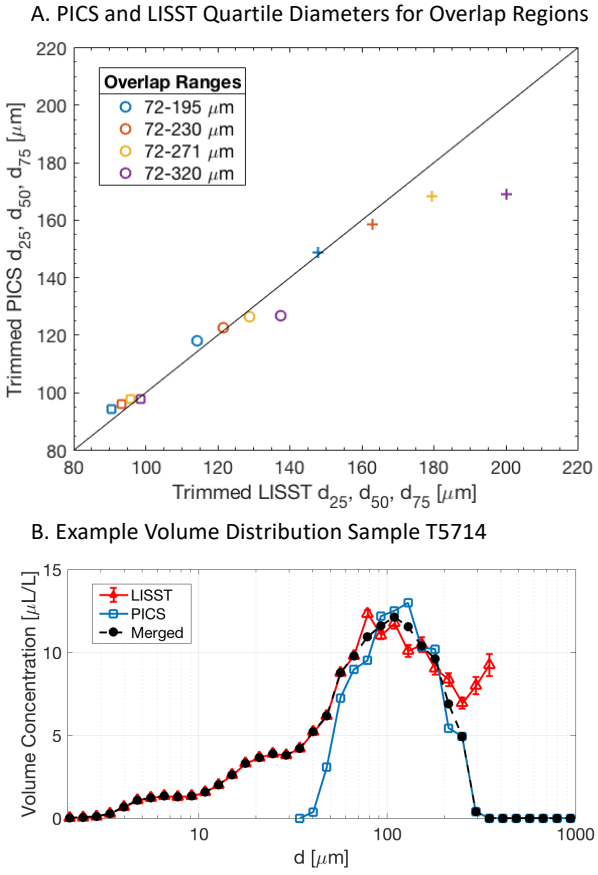

Figure 3: An example of merging LISST-100X and PICS size distributions. Following Mikkelsen et al., 2005, particle size quartiles, d_{25},d_{50}, and d_{75}, were compared between the instruments over "trimmed" or overlap size bins. For each sample, a correction factor was determined by calculating the average ratio of LISST volume concentration (µL/L) to PICS volume (mm^3) for bins a defined overlap region.(A) shows an example comparing the quartiles a given sample over size bin groups in this range: 23-31 (purple), 23-30 (yellow), 23-29 (red), and 23-28 (blue). The black line represents the 1:1 line. In this example, the best agreement is over bins 23-29 which covers particle sizes 73-230 µm. (B) shows the resulting distribution.

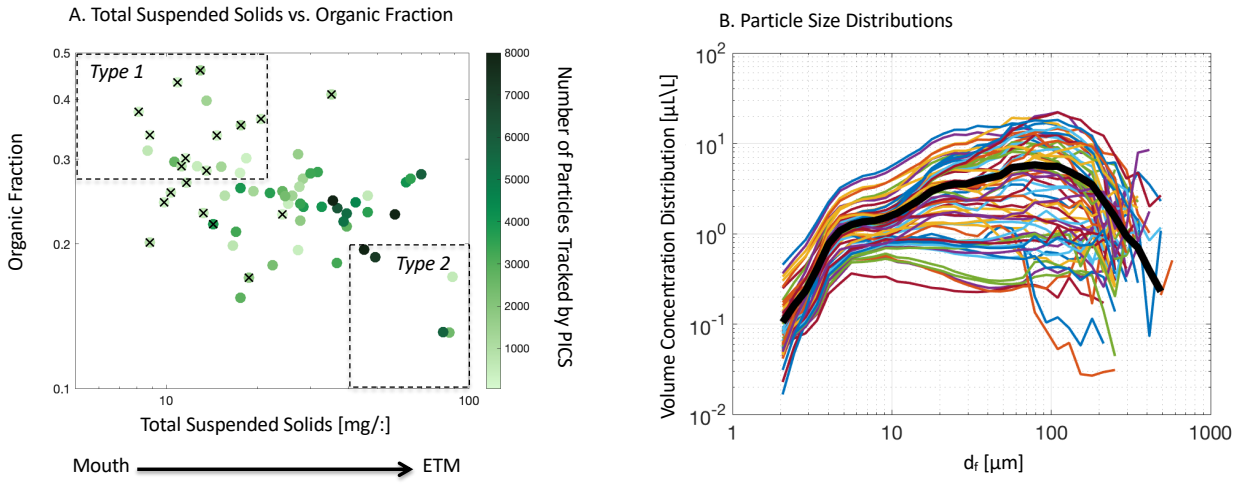

Figure 4: (A) Total suspended solids versus organic fraction from pump samples collected in the York River Estuary. Symbol color indicates the number of particles tracked by the PICS in each sample. Black "x" indicates stations that could not be fit with a realistic F (i.e. F<1, F>3, or σ_F>0.2). Type 1 and Type 2 suspensions are marked out by dashed lines. (B) LISST+PICS merged particle size distributions from samples collected in the York River Estuary. The solid black line represents the average particle size distribution.

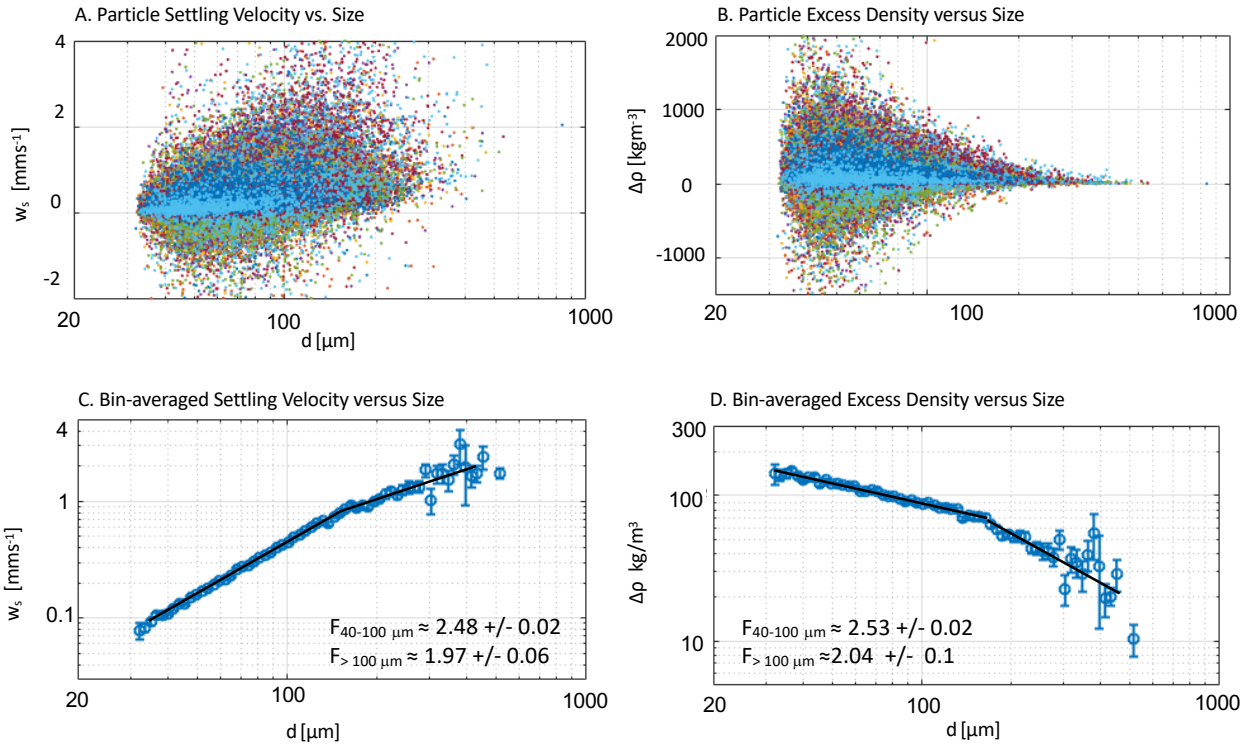

Figure 5: PICS measured size (d_f) versus settling settling velocity (w_s), and (B) calculated excess density ($\Delta\rho$) for all particles tracked. Average w_s (C) and $\Delta\rho$ (D) over **75 logarithmically** spaced particle size bins from 30-1000 µm. Best fit fractal models indicated with black lines.

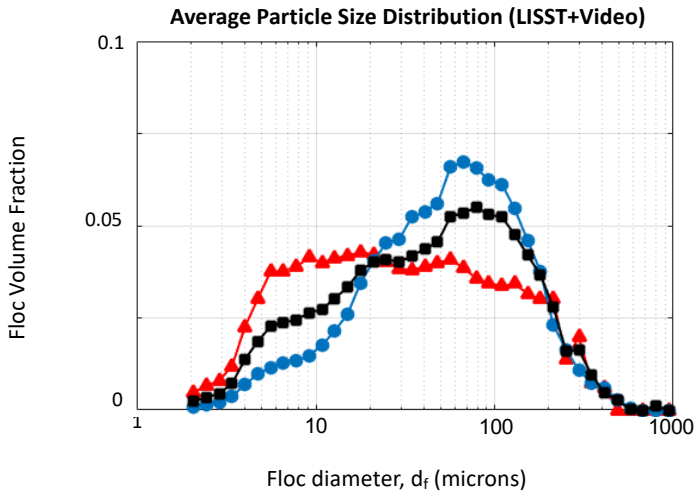

Figure 6: Average particle size distributions, in terms of volume fraction, for all samples (black), samples with Low F_{org}, High TSS (Type 2, blue) and samples with High F_{org}, Low TSS (Type 1, red).

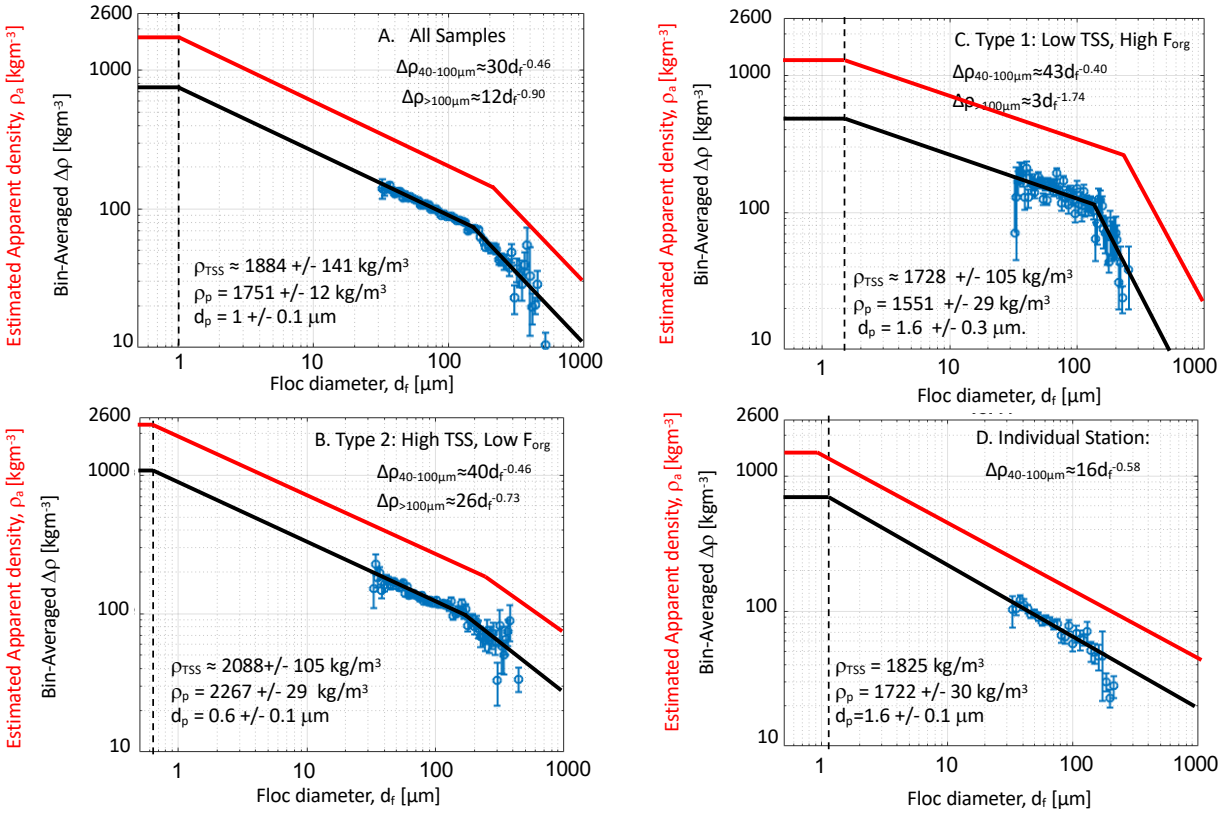

Figure 7: Bin averaged $\Delta\rho$ versus d_f for (A) All tracked particles, (B) Type 1 suspensions, (C) Type 2 suspensions, and (D) an individual station. All cases were averaged over logarithmically spaced size class bins from d_f=30-1000 μm. Figures A,B,C show results average over 75 bins and D shows results over 30 bins. The red and black lines shows ρ_a and excess $\Delta\rho$ assuming a fractal model. The theoretical relationship between the two was used to estimate ρ_p and d_p. Fractal models were evaluated using ρ_p inferred from pump samples (ρ_{tss})

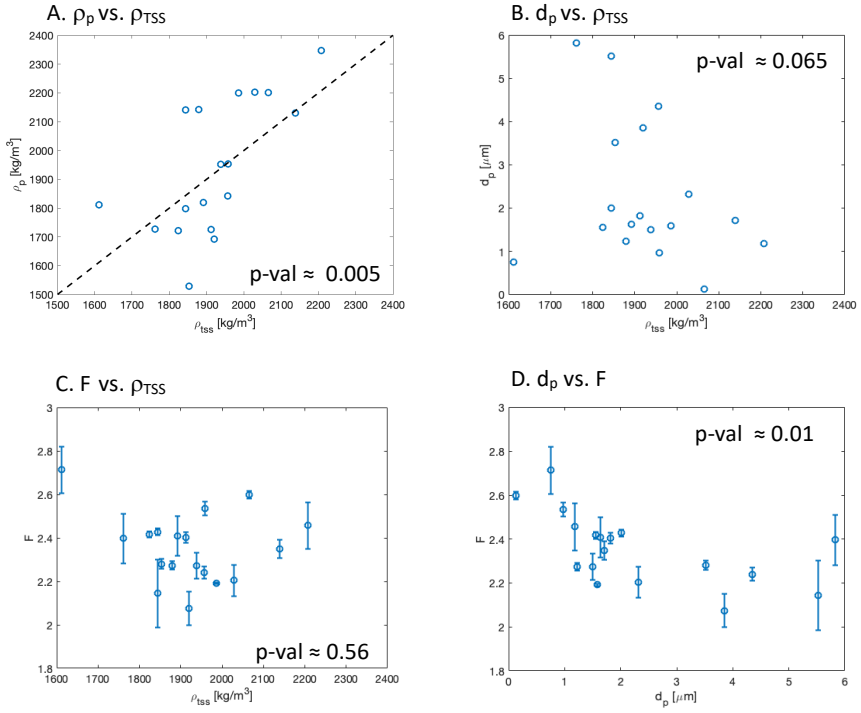

Figure 8: Theoretical relationship between apparent (ρ_a) and excess ($\Delta\rho$) density applied to individual stations. PICS fractal models were "confidently" fit to 18 stations. Solid line on (A) is the 1:1 line between best fit ρ_p and observed ρ_{TSS}.

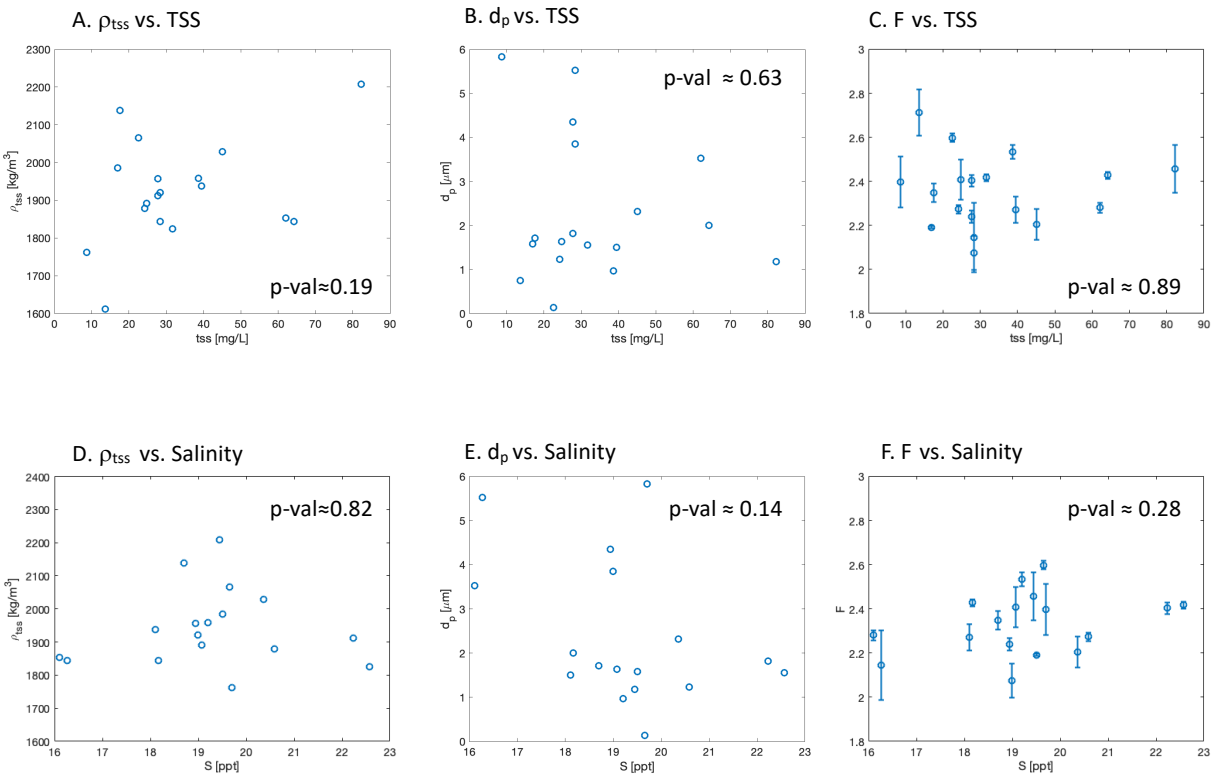

Figure J: Influence of total suspended solids (TSS), salinity and current velocity (U) on fractal (F) and primary particle properties (ρ_{tss} and d_f).

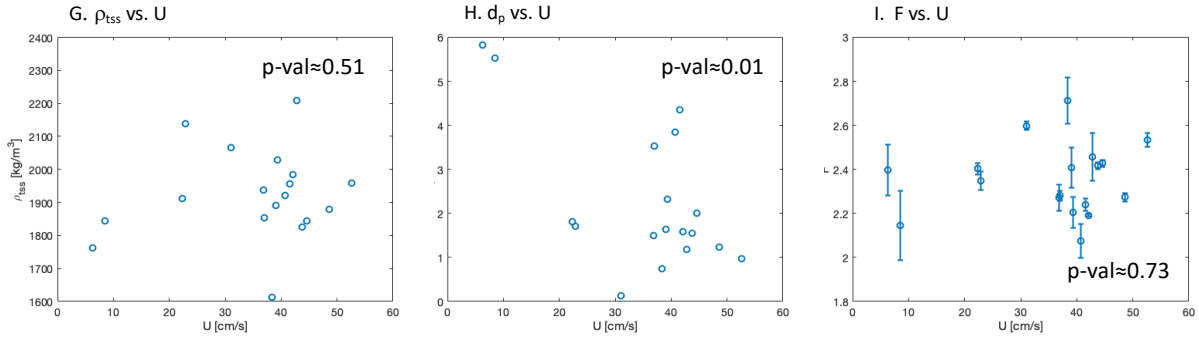

Figure 9: Influence of total suspended solids (TSS), salinity and current velocity (U) on fractal (F) and primary particle properties (ρ_{tss} and d_f).

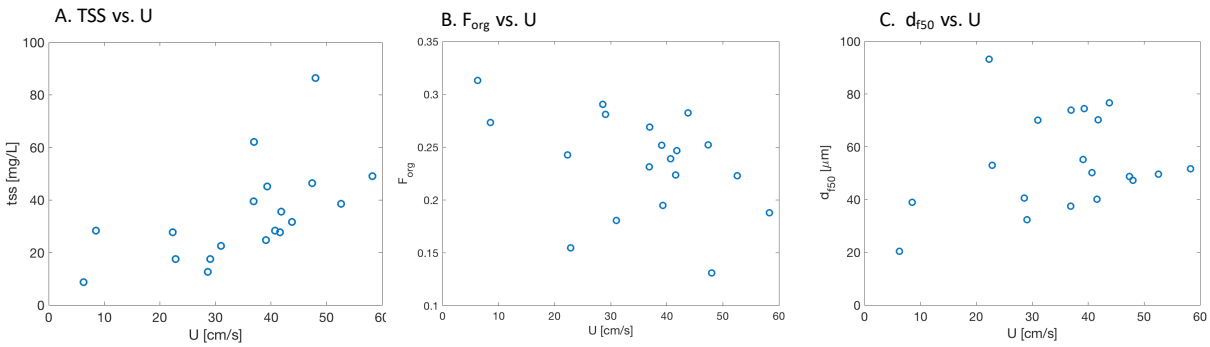

Figure 10: Influence of current velocity (U), or total suspended sediment concentrations (TSS), fraction organic (F_{org}) and median particle size by volume (d_{50v}).